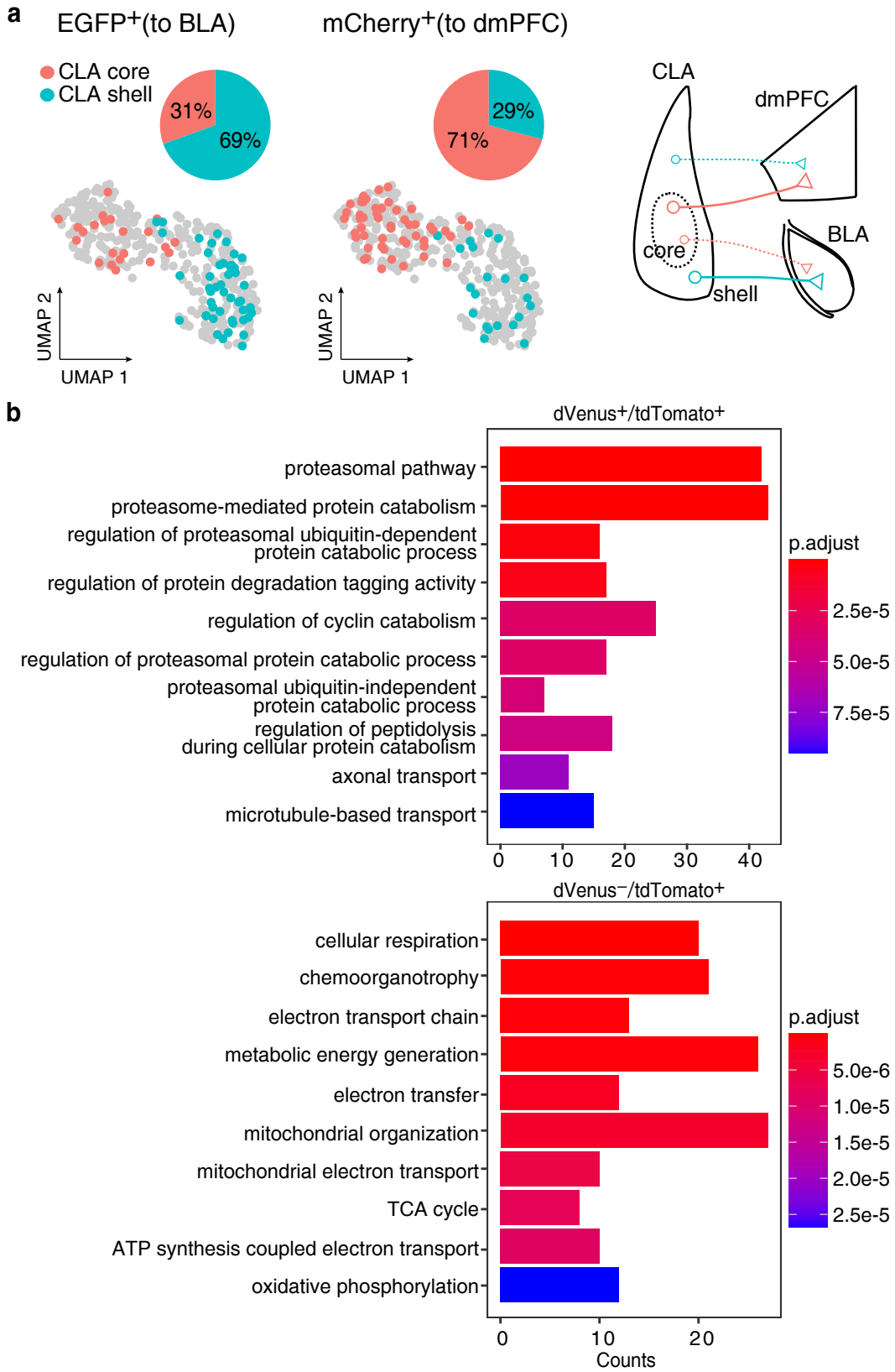

Extended Data Fig. 1. Projectional and functional diversity of CLA neurons. (**a**) Distribution of projection-defined CLA neurons in the core–shell transcriptomic space. Retrogradely labeled dmPFC-projecting neurons (mCherry$^+$) were enriched in the core, whereas BLA-projecting neurons (EGFP$^+$) were enriched in the shell. (**b**) Gene ontology (GO) term enrichment analysis for differentially expressed genes between dVenus$^+$/tdTomato$^+$ and dVenus$^-$/tdTomato$^+$ neurons. dVenus$^+$/tdTomato$^+$ neurons showed enrichment in proteasome-related and axonal transport pathways, while nonresponsive neurons were enriched in mitochondrial respiration and energy metabolism.

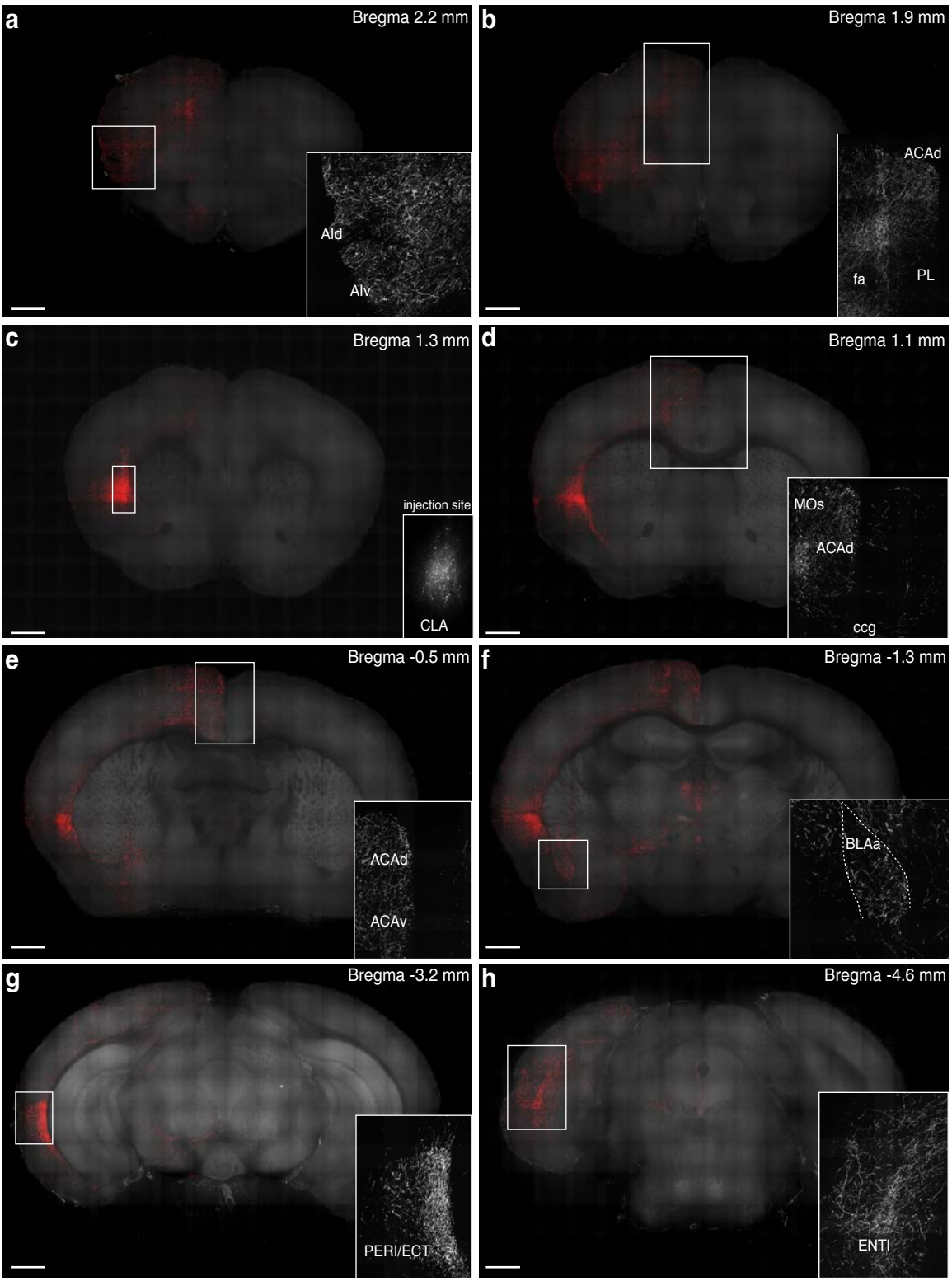

Extended Data Fig 2. Representative images of CLA^{Car12+} axon labeling. (a to h) Coronal sections showing palmitoylated mScarlet-labeled axons arising from CLA^{Car12+} neurons after viral injections into the CLA (c, inset). Bregma coordinates are indicated avove each panel. Dense axonal projections are observed in the agranular insular cortex, dorsal and ventral parts, (AId, AIv; a), dorsal and ventral anterior cingulate cortex (ACAd, ACAv; d and e), secondory motor cortex (MOs; d), and anterior basolateral amygdala (BLAa; f), perirhinal and ectorhinal cortex (PERI/ECT; g), and lateral entorhinal cortex (ENTl; h). Scale bars, 1 mm. White boxes in the low-magnification images indicate the regions shown at higher magnification in the corresponding insets.

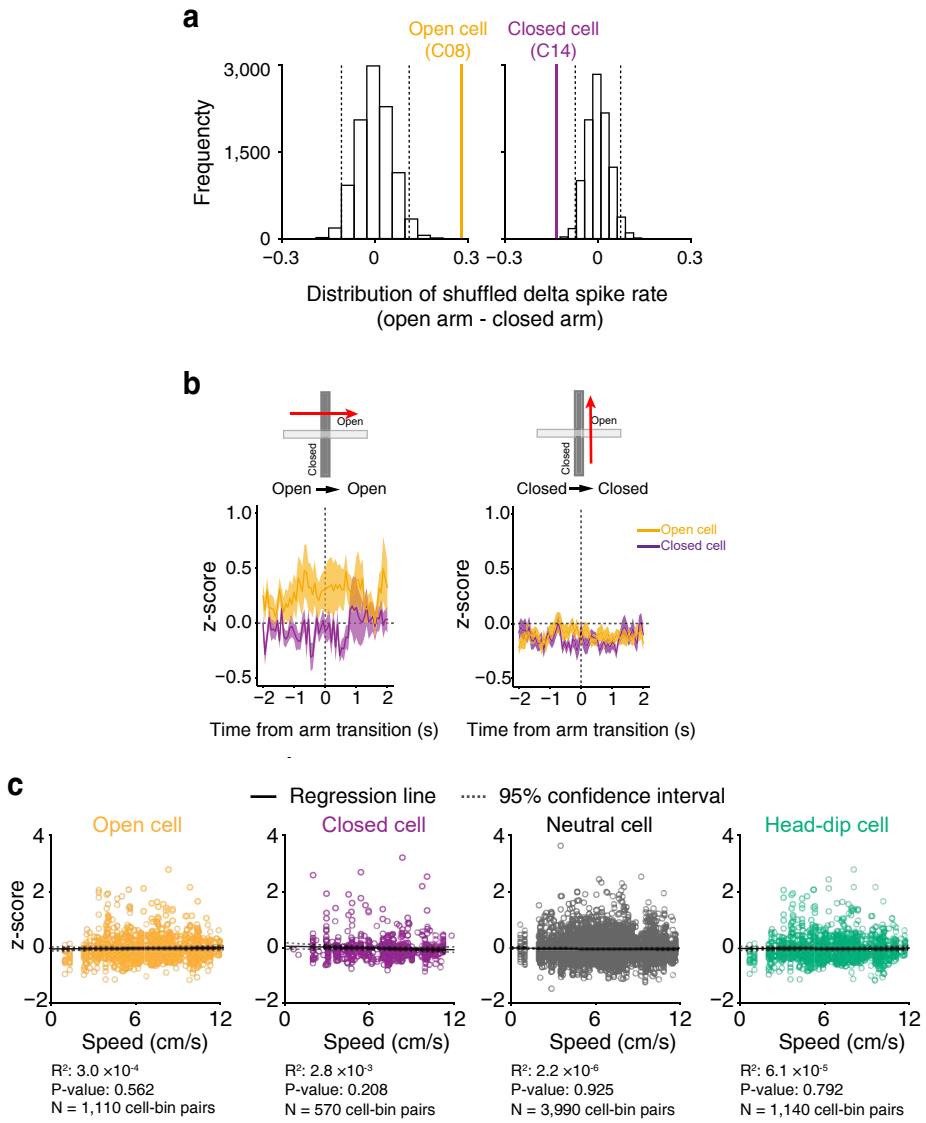

Extended Data Fig 3. Control analyses for CLA^{Car12+} vigilance coding in the EPM. (**a**) detection of arm-selective cells. Histograms show the null distribution of the difference in inferred spike rate between open and closed arms obtained from 10,000 label shuffles. Dotted lines mark ± 2 s.d. of the shuffled distribution. Orange and purple lines indicate the true open-closed difference for a representative open cell (C08) and closed cell (C14), respectively. (**b**) Same-arm transition control. Z-scored ΔF/F traces of open (orange) and closed (purple) cells aligned to transitions between two open arms (left) or two closed arms (right). Thick lines donate the mean ± s.e.m.; shaded areas, s.e.m. Epoch$_{O\text{-}O}$= 5 times, Epoch$_{C\text{-}C}$= 31 times. (**c**) Velocity control. Scatter plot of mouse velocity versus Z-scored ΔF/F for open (orange), closed (purple), neutral (gray), and head-dip (green) cells, binned at 10 s. Solid lines are best-fit regressions; dotted lines, 95% confidence interval. Correlation coefficients did not differ from zero for any group ($p > 0.2$).

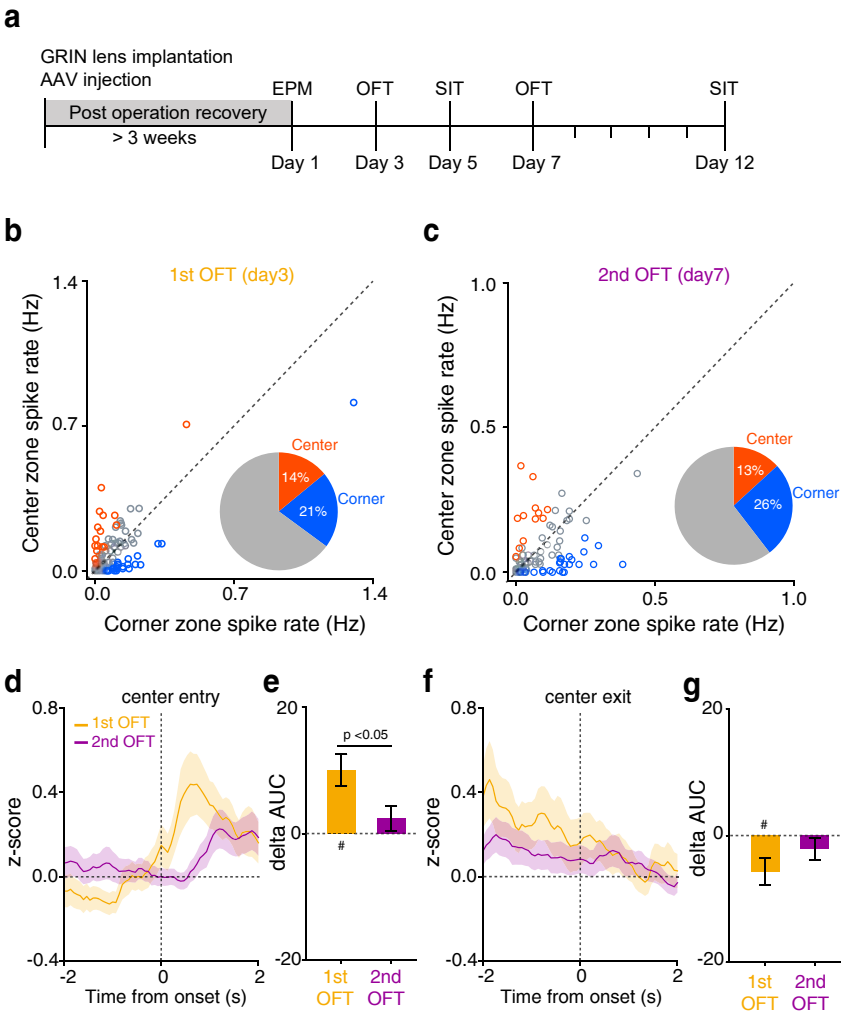

Extended Data Fig 4. Control sessions without SDS exposure for CLA^{Car12+} in the OFT. (**a**) Experimental design for in vivo Ca^{2+} imaging from CLA^{Car12+} neurons across the elevated plus maze (EPM), open-field test (OFT), and social interaction test (SIT). (**b and c**) Scatter plot showing inferred spike rates of individual CLA^{Car12+} neurons in the center versus corner zones of the 1st OFT (b) and 2nd OFT (c). Orange and blue circles indicate center and corner cells, respectively. Inset pie chart summarizes the proportion of each cell type. 1st-OFT, N_{cells} = 114 from 3 mice; 2nd-OFT N_{cells} = 91 from 3 mice. (**d to g**) Z-score traces (D and F) and delta AUC (0 to +2 s minus −2 to 0 s; e and g) of center cells aligned to transitions: center entry (d and e) and center exit (f and g) in 1st-OFT (orange) and 2nd-OFT (purple). Lines represent mean activity; shaded areas, s.e.m.; Mean ± s.e.m.; $Epoch_{1stOFT\text{-}entry}$ = 28 times, $Epoch_{2ndOFT\text{-}entry}$ = 53 times, $Epoch_{1stOFT\text{-}exit}$ = 30 times, $Epoch_{2ndOFT\text{-}exit}$ = 52 times. *P* values by unpaired *t*-test. $^{\#}P < 0.05$ for AUC comparison between −2 to 0 s and 0 to +2 s by paired *t*-test.

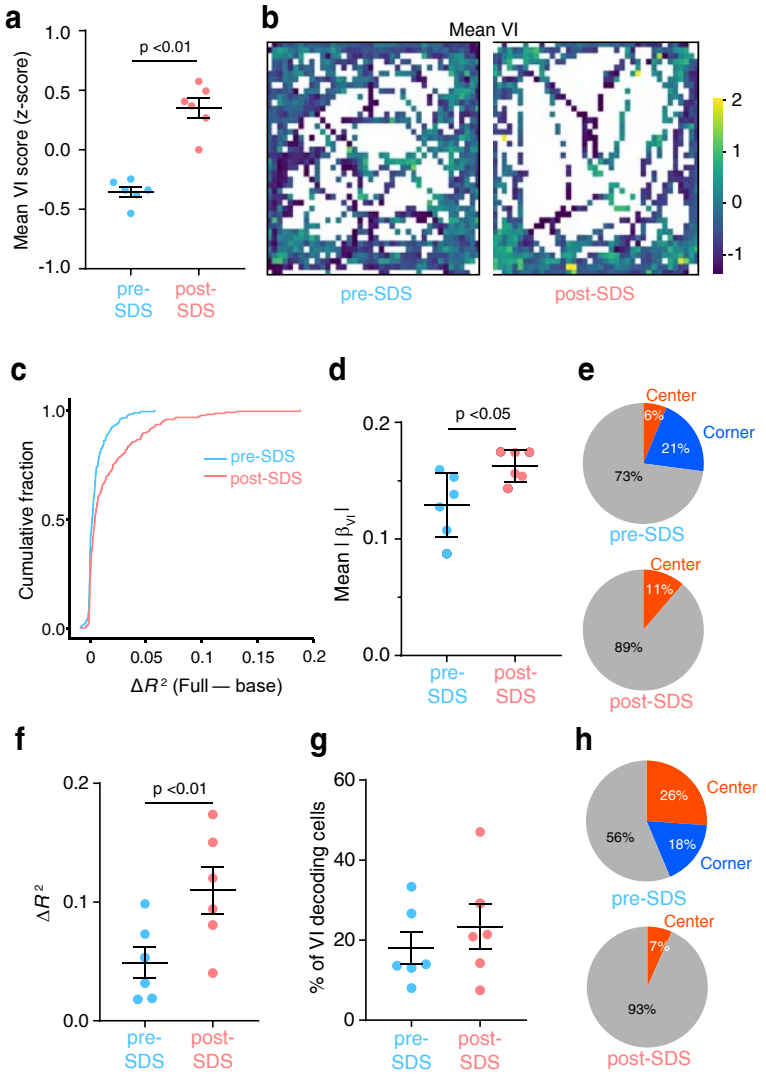

Extended Data Fig 5. Vigilance index dynamics and neural representations before and after SDS in the OFT. (**a**) Behavioral validation of the vigilance index (VI). Mean VI score (z-scored; unified PC1) for each mouse in the pre-SDS (blue) and post-SDS (pink) sessions. Mean ± s.e.m, *P* value by paired *t*-test. (**b**) Representative spatial maps of the VI in the pre-SDS (left) and post-SDS (right) sessions, displayed using a shared color scale. (**c to e**) GLM-based encoding of VI. Cumulative distributions of ΔR^2 (c) and mean regression coefficient magnitude (d) for pre-SDS and post-SDS sessions; Mean ± s.e.m, *P* value by paired *t*-test. Composition of VI cells across zone-selective classes (center, corner, and neutral) in pre-SDS and post-SDS sessions (e). (**f to h**) Population-level decoding of VI. Cross-validated ΔR^2 (real R^2 minus shuffle mean) (f) and proportion of neurons with significant contributions to VI score decoding (g) in pre-SDS and post-SDS sessions. Mean ± s.e.m, *P* value by paired *t*-test. Composition of neurons with significant contributions to VI score decoding across zone-selective classes in pre-SDS and post-SDS sessions (h).

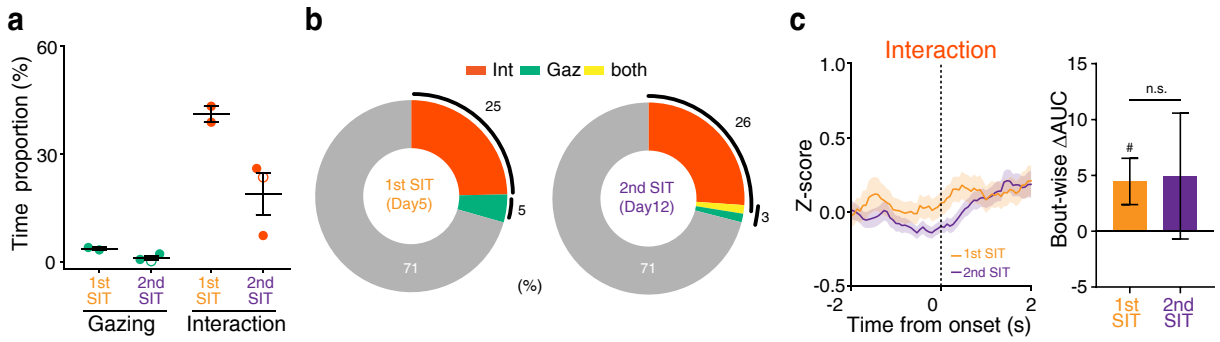

Extended Data Fig 6. Control SIT sessions without SDS exposure for CLA^{Car12+} neurons. (**a**) Time proportion spent in gazing and interaction during the first and second social interaction tests (SIT) performed without repeated social defeat stress (n = 3 mice). Three mice were tested; one (open circles) was excluded because it entered an area outside the predefined arena during the 1st SIT. (**b**) Donut charts show fractions of interaction (orange), gazing (green), both (yellow), and neutral (gray)-classified CLA^{Car12+} cells in the 1st (left panel) and 2nd (right panel) SIT sessions. 1st-SIT, N_{cells} = 85 from 2 mice; 2nd-SIT N_{cells} = 69 from 2 mice. (**c**) Event-aligned z-scored Ca^{2+} activity to interaction onset (left panel) and response magnitude quantified as bout-wise ΔAUC ($AUC_{0\ to\ +2\ s}$ minus $AUC_{-2\ to\ 0\ s}$; right panel) in the first and second SIT sessions. $Epoch_{1stSIT\text{-}interaction}$ = 26 times, $Epoch_{2ndSIT\text{-}interaction}$ = 24 times. Lines indicate mean; shaded areas, s.e.m.; Mean ± s.e.m.; n.s. not significant between sessions performed by Student' s *t*-test. $^{\#}P < 0.05$ for within-session ΔAUC comparison between −2 to 0 s and 0 to +2 s by paired *t*-test.

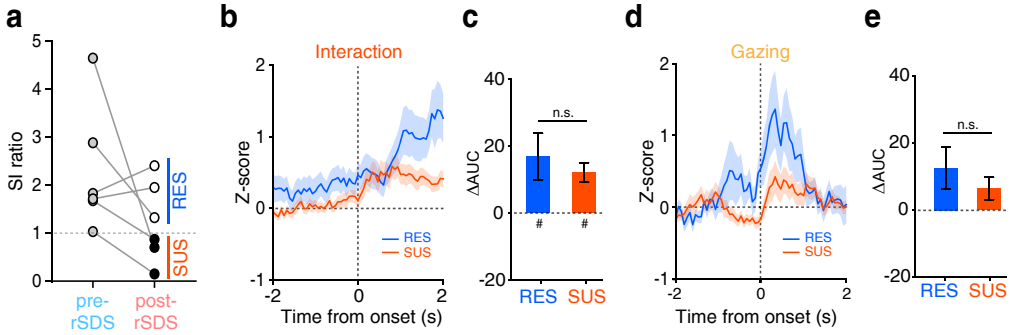

Extended Data Fig 7. Coping style does not modulate event-locked responses of CLA^{Car12+} neurons in the SIT. (**a**) Social interaction (SI) ratio of the post-rSDS was used to classify mice as resilient (RES; SI ≥ 1, blue) or susceptible (SUS; SI < 1, orange). Lines connect paired measurements from the same mouse. (**b and c**) Interaction-aligned mean z-scored Ca^{2+} signals (b) and event-locked response magnitude (c), quantified as ΔAUC (0 to 2 s minus −2 to 0 s), for interaction cells in RES and SUS mice. $^{\#}P < 0.05$ vs. baseline within group (0 to +2 s vs. −2 to 0 s) by paired *t*-tests. (**d and e**) Gazing-aligned mean z-scored Ca^{2+} signals (d) and ΔAUC (e) of gazing cells in RES and SUS mice. Mean ± s.e.m. n.s., not significant between groups by unpaired *t*-test.

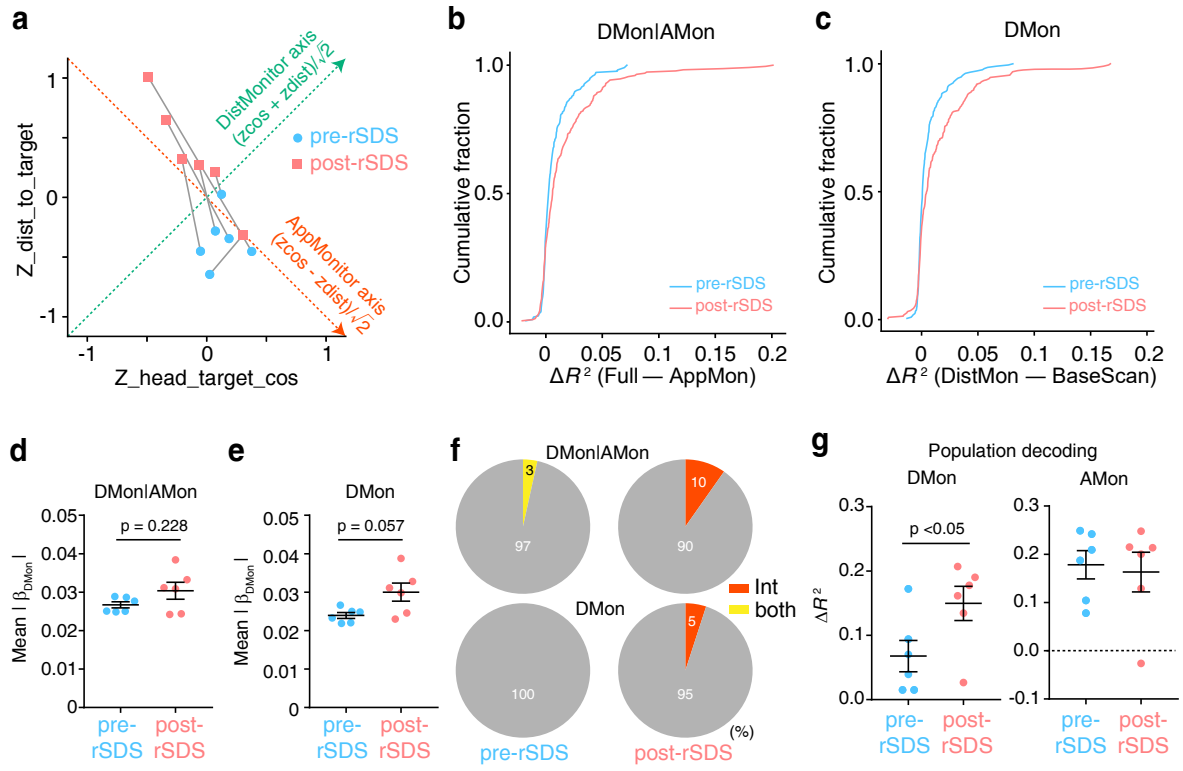

Extended Data Fig 8. Stress-dependent modulation of orthogonal target-monitoring axes in the SIT. (**a**) Mouse-level visualization of target-monitoring variables in the z-scored space defined by distance to target (z_dist_to_target) and head-direction-to-target cosine (z_head_target_cos). Data from the six mice used in the SIT analysis are shown for pre-rSDS (blue) and post-rSDS (pink) sessions. Gray lines connect paired values from the same mouse. This feature space is also shown with two orthogonal target-monitoring axes used in the regression analysis: distance-maintaining monitoring (DistMonnitor, green arrow) and approach-linked monitoring (AppMonitor, orange arrow). (**b and c**) Empirical cumulative distributions of cross-validated ΔR^2 attributable to DMon|AMon (b) and DMon alone (c), shown for pre-rSDS (blue) and post-rSDS (pink) sessions. (**d and e**) Mouse-level mean magnitude of the DMon regression coefficient for DMon|AMon (d) and DMon alone (e) in the pre-rSDS and post-rSDS sessions. Mean ± s.e.m, *P* value by paired *t*-test. (**f**) Pie charts show the proportions of interaction-selective (int, orange), dual-selective (both, yellow; interaction and gazing), and neutral (gray) cells in the DMon-significant cells for DMon|AMon (upper) and DMon (bottom) models in both pre-rSDS (left) and post-rSDS (right) conditions. (**g**) Population-level decoding of DMon (left) and AMon (right) from CLA^{Car12+} ensemble activity. Cross-validated ΔR^2 (real R^2 minus shuffle mean) . Mean ± s.e.m. Dashed line at 0 indicates the shuffle mean. Mean ± s.e.m, *P* value by paired *t*-test.